frontiers | Frontiers in Soil Science

TYPE Original Research
PUBLISHED 08 August 2025
DOI 10.3389/fsoil.2025.1617526

OPEN ACCESS

EDITED BY
Bifeng Hu,
Jiangxi University of Finance and Economics, China

REVIEWED BY
Luigi Jovane,
University of São Paulo, Brazil
Lei Lu,
Hunan Agricultural University, China

*CORRESPONDENCE
Lucas Pereira Leão
lucas.leao@ufop.edu.br

RECEIVED 30 April 2025
ACCEPTED 08 July 2025
PUBLISHED 08 August 2025

CITATION
Pantuzzo FL, Laureano FV, Cabral CL, Salomão GN, Dall'Agnol R, Pimenta VB and Leão LP (2025) Rapid and low-cost geochemical indices for tracing iron mining tailings within fluvial sediments: a case study from the Paraopeba River after the B1 Dam burst in Brumadinho, Minas Gerais, Brazil. *Front. Soil Sci.* 5:1617526.
doi: 10.3389/fsoil.2025.1617526

Rapid and low-cost geochemical indices for tracing iron mining tailings within fluvial sediments: a case study from the Paraopeba River after the B1 Dam burst in Brumadinho, Minas Gerais, Brazil

Fernando Luís Pantuzzo[1], Fernando Verassani Laureano[2], Caíque Lima Cabral[3,4], Gabriel Negreiros Salomão[5], Roberto Dall'Agnol[5], Vitor Brognaro Pimenta[2] and Lucas Pereira Leão[6]*

[1]SRK Consulting, Belo Horizonte, Brazil, [2]Vale S.A., Belo Horizonte, Brazil, [3]Arcadis, Belo Horizonte, Brazil, [4]Departament of Geology, Federal University of Rio de Janeiro, Rio de Janeiro, Brazil, [5]Instituto Tecnológico Vale, Belém, Brazil, [6]Departament of Geology, School of Mines, Federal University of Ouro Preto, Ouro Preto, Brazil

The B1 dam failure at Córrego do Feijão mine in Brumadinho (Minas Gerais, Brazil) in January 2019 caused severe and long-lasting environmental impacts, particularly on the fluvial sediments of the Paraopeba River basin. Characterizing the geochemical signature of the iron tailings and, especially, distinguishing these materials from the river's natural sediments remains a significant challenge. In this context, the present study investigates the geochemical signatures of major and minor elements in sediments affected by the tailings and proposes a set of geochemical indices capable of identifying the presence of tailings in impacted sediments. Six cores from a drilling program were extracted along the Paraopeba River bedload. A total of 54 samples were collected, and subsequently subjected to X-ray fluorescence analysis to determine the major and minor elements (Al_2O_3, CaO, Fe, MgO, Mn, P, SiO_2, and TiO_2). The main constituents in natural sediment samples were SiO_2 and Al_2O_3, which together accounted for 52.7% to 96.6%, while Fe_2O_3 represented 1.1% to 42.7%. Conversely, in tailings samples, Fe_2O_3 concentrations ranged from 36.6% to 88.8%, followed by silica (8.4% to 34.4%) and alumina (0.87% to 19.1%). Fe_2O_3 levels were above 60% in most of the tailing's samples. Natural sediment samples generally had higher TiO_2, CaO, and MgO content than tailings samples, which, in turn, showed generally higher levels of MnO and P_2O_5. Based on the aforementioned data, we proposed two chemical compositional indices, IRS1 and IRS2, which are rapid and low-cost to calculate. Due to the compositional characteristics of tailings and sediments, IRS values spread on an opposite diagonally shape when dispersed on a binary IRS1 x IRS2 graph. The pair of indices was applied to stream sediment samples from the Paraopeba River, collected in 2019 as part of the Emergency Monitoring Program. The results indicated that samples classified as tailings were concentrated upstream of the UTE Igarapé reservoir spillway, reinforcing the importance of the reservoir in reducing the propagation of tailings along the Paraopeba River channel. Moreover, when the indices are applied to stream

sediment samples collected in 2023 from affected areas where tailings have been subjected to dredging activities, low IRS1 and IRS2 values are observed. Thus, considering the large amount of data generated by the sediment monitoring activities in the Paraopeba River basin, the proposed indices serve as a graphical tool for tracking the dispersion of tailings on a spatial and temporal scale.

KEYWORDS

fingerprints, tailings, Paraopeba River, river sedimentation, dam failure

1 Introduction

Mining has long been, and continues to be, a fundamental sector of economic activity, supplying essential raw materials for human development. However, the generation of mine tailings — comprising crushed rock debris and mineral processing fluids — has become one of the largest sources of industrial waste globally (1, 2). Tailings dams are necessary infrastructures in mining operations, yet their structural failures can result in severe and widespread environmental, economic, and human health consequences (3, 4).

Among the various environmental compartments affected by such disasters, river sediments are particularly impacted. These sediments serve as natural archives of catchment-scale environmental conditions, but the passage of tailings waves can bury or erode these records, disrupting sedimentary and geochemical dynamics (5, 6). Furthermore, as major geochemical reservoirs, river sediments play a crucial role in the long-term retention, mobilization, and redistribution of metals and other contaminants due to their adsorption, absorption, and desorption capacities (7–9). Understanding the alterations in sediment geochemistry following tailings dam failures is therefore essential for assessing environmental impacts, guiding monitoring efforts, and informing remediation strategies.

Widely found in the literature, sediment provenance studies have been performed with a range of purposes (e.g., sedimentary basin analysis, mineral and oil exploration, and contaminant dispersion and risk assessment). For environmental purposes, provenance studies may use different tracers, such as mineral content (10, 11), geochemical ratios and properties (9, 12), statistics of metal concentrations (13) and isotopic ratios (6, 14, 15). The term fingerprint is used when a particular property of a specific source can be used to relate it with sediments (or contaminants), and this approach has proven useful for aqueous system conservation and restoration (16, 17).

On January 25, 2019, the B1 Dam, located in the municipality of Brumadinho, Minas Gerais state of Brazil, collapsed. This failure generated a high-energy gravitational mass movement that flowed down the valley of Ferro-Carvão Creek before it reached the Paraopeba River (Figure 1), where the material was deposited as a low-energy mudflow (5). Once in the river channel, the tailings began to be transported downstream as washed, suspended and bedload materials, and local mixing with natural sediments also occurred. A comparison of the previous topography and the modified topography yielded an estimate of 9.7 Mm^3 of total waste overflow (19). Approximately 8.1 Mm^3 was deposited in the valley of Ferro-Carvão Creek, and 1.6 Mm^3 settled into the Paraopeba River. In addition to socioeconomic impacts and those associated with fauna and flora, studies have indicated that the water quality and fluvial sediments in the Paraopeba River Basin were affected (12, 20, 21). On the other hand, studies have argued that the medium- and long-term impacts on Paraopeba River water and sediment quality are not as great as initially expected, given the geological background and previous land use within its catchment (22–24). Therefore, establishing a clear causal link between geochemical anomalies and the presence of tailings is mandatory for precise environmental impact assessment.

Pacheco et al. (25) highlights the importance of understanding the impacts resulting from tailings dam failures and emphasize the need for long-term environmental monitoring, noting that such efforts are uncommon due to their high cost. For the assessment of the impacts of tailings in the affected areas, a clear distinction between the sediments accumulated in the Paraopeba Basin before the collapse of the B1 dam and the tailings related to it is essential. Furthermore, it should be achieved in a fast, low-cost and precise approach to support the urgency and responsibility associated to the decision making during the restoration processes. Laureano et al. (11) aimed to differentiate between tailings and sediments based on textural, mineralogical, and physical characteristics. The results indicate that natural sediments deposited in the Paraopeba River predominantly consist of kaolinite, quartz, and quartz + hematite as the main mineral assemblages. In contrast, the tailings from the B1 dam are primarily composed of hematite, with occasional occurrences where hematite + kaolinite dominate.

However, the geochemical characterization of these different materials is necessary to add additional criteria for their individualization. This is particularly relevant because there is evidence of local mixing between these two components. In this work, we present the results of whole-rock analysis of major and minor elements in tailings and sediments and develop a pair of geochemical indices that are calculated from these data that are capable of distinguishing natural sediments from tailings released

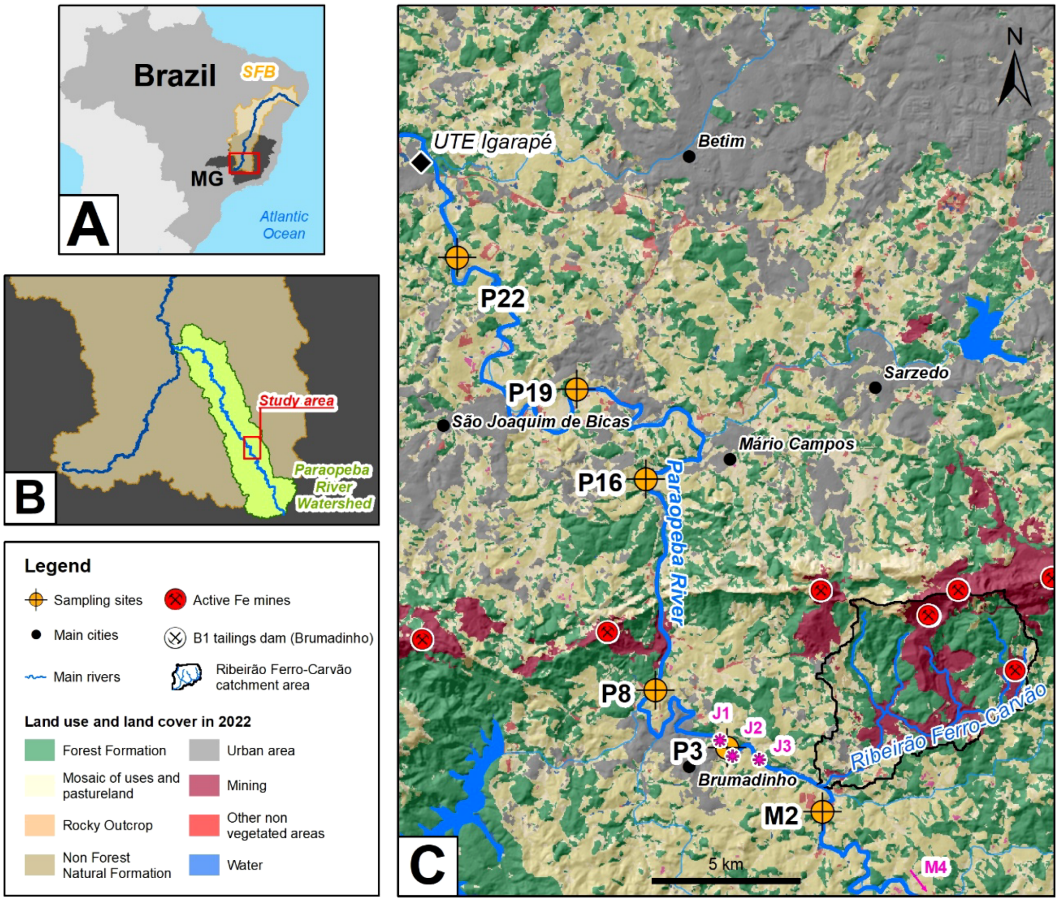

FIGURE 1
Location map of the study area in the state of Minas Gerais (MG), southeastern Brazil **(A)**. The area is located in the Paraopeba River watershed, upper part of the São Francisco Basin (SFB) **(B)**. The locations of the sediment cores sampled in 2019 are presented over the land use and land cover **(C)** layers of the area. Source: **(C)** modified from the MapBiomas Amazonia Project, 2022. M4, J1, J2 and J3 are sampling points from Silva et al. (18), the results of which are discussed later.

from the B1 Dam. A graphical dispersion tool is also suggested to enhance visualization in terms of geochemical concentrations and provenience and spatiotemporal evolution, as sediments and tailings are influenced by fluvial processes.

2 Study area

The Paraopeba River, a major tributary of the São Francisco River, is an important Brazilian waterway. The watershed is elongated, spanning approximately 537 km in length and covering an area of 12,091 km^2. It encompasses 48 municipalities home to more than one million inhabitants (26). Economic activities include mining, metallurgy, and agriculture. These sectors, and hydropower plants for energy generation, constitute the primary consumers of water from the Paraopeba River (27).

The watershed features a complex geological setting that evolved mostly during the Archean and Paleoproterozoic eras of Precambrian Earth's history. Mafic and ultramafic rocks belonging to the Archean Rio das Velhas greenstone occur in the higher sectors of the Paraopeba River basin (28). Paleoproterozoic metasedimentary units such as quartzites, phyllites, dolomites and banded iron formation belonging to the Minas Supergroup crop out in the higher and middle course sectors (29). Neoproterozoic sedimentary cover belonging to the Bambuí Group comprises the substrate in the lower sector (30). The crystalline basement is composed of tonalitic to granitic polydeformed gneissic rocks throughout the upper and middle sectors of the basin (31).

The Paraopeba watershed is located in the Iron Quadrangle (32), a classic mining province rich in diverse mineral deposits, where mining activities have been documented since the 17th century, during the Brazilian colonial period. The abundance of metallic ores is attributed to the occurrence of low-grade metamorphic processes coupled with intense hydrothermal activity (32). After historical cycles of gold extraction, large iron deposits related to Precambrian banded iron formations (itabirites), predominantly composed of iron oxides (e.g., hematite and magnetite) and quartz (33), became the dominant exploited ore.

TABLE 1 Whole-rock chemical analyses and true density of tailings and natural sediments from the Paraopeba River, 2019 drilling campaign (data from 11).

Core	Interval (cm)	Class	Al_2O_3 (%)	CaO (%)	Fe_2O_3 (%)	MgO (%)	MnO (%)	P_2O_5 (%)	SiO_2 (%)	TiO_2 (%)	LOI (%)	True Density (g/cm^3)
M2-01	01-04	Natural	26.30	0.36	17.44	0.49	0.37	0.17	39.86	0.97	14.94	2.57
M2-02	20-30	Natural	26.79	0.34	17.65	0.48	0.42	0.17	39.02	0.93	14.78	2.69
M2-03	40-48	Natural	20.29	0.31	19.10	0.42	0.36	0.14	48.67	0.86	10.75	2.77
M2-04	60-68	Natural	18.12	0.27	19.90	0.40	0.43	0.16	50.06	0.80	10.22	2.77
M2-05	84-90	Natural	6.41	0.18	14.85	0.26	0.09	0.05	74.12	0.61	2.64	2.82
M2-06	100-106	Natural	9.57	0.16	24.87	0.35	0.16	0.06	59.91	0.72	4.36	2.95
M2-07	120-126	Natural	5.43	0.14	29.27	0.24	0.13	0.05	61.71	0.54	2.37	3.05
M2-08	140-146	Natural	10.07	0.13	41.10	0.21	0.34	0.07	42.61	0.63	5.30	3.23
M2-09	160-166	Natural	4.18	0.11	11.86	0.15	0.09	0.03	80.65	0.42	1.72	2.81
M2-10	184-190	Natural	2.47	0.09	1.10	0.10	0.01	0.01	94.06	0.19	0.75	2.68
P3-01	04-10	Tailing	2.20	0.06	72.85	< 0.033	0.35	0.09	22.38	0.10	1.62	4.04
P3-02	24-30	Tailing	2.88	0.07	67.87	< 0.033	0.35	0.09	26.66	0.13	1.79	3.89
P3-03	44-48	Tailing	1.82	0.05	76.73	< 0.033	0.33	0.08	19.18	0.10	1.37	4.21
P3-04	60-64	Tailing	0.94	0.04	83.93	< 0.033	0.32	0.08	13.47	0.08	1.04	4.36
P3-05	86-90	Tailing	5.91	0.09	63.40	0.09	1.49	0.23	23.92	0.20	4.71	3.78
P3-06	106-110	Tailing	3.15	0.07	62.56	< 0.033	0.59	0.12	30.46	0.14	2.59	3.75
P3-07	124-130	Tailing	4.81	0.09	60.45	0.08	1.13	0.20	28.85	0.16	4.17	3.69
P8-01	04-08	Tailing	3.55	0.08	74.67	< 0.033	0.70	0.13	17.58	0.14	2.82	4.13
P8-02	12-16	Tailing	0.87	0.05	88.72	< 0.033	0.41	0.08	8.44	0.07	1.17	4.67
P8-03	26-30	Tailing	5.85	0.10	62.75	0.07	1.58	0.26	24.38	0.18	4.78	3.80
P8-04	44-50	Tailing	6.83	0.11	63.39	0.11	1.79	0.29	22.31	0.21	5.42	3.76
P8-05	66-72	Tailing	11.30	0.14	62.37	0.22	3.38	0.52	13.03	0.32	9.16	3.68
P8-06	86-92	Tailing	11.29	0.14	62.62	0.23	3.42	0.56	12.24	0.31	9.57	3.68
P8-07	98-104	Natural	17.04	0.24	20.56	0.43	0.31	0.17	51.27	0.75	9.52	2.81
P8-08	108-114	Natural	9.27	0.21	24.15	0.30	0.21	0.09	60.22	0.82	4.69	2.94
P8-09	130-134	Natural	5.25	0.17	5.32	0.20	0.07	0.04	84.71	0.33	1.65	2.71
P8-10	150-156	Natural	14.22	0.31	16.85	0.38	0.26	0.12	57.70	0.69	9.60	2.73
P16-01	04-10	Tailing	10.48	0.15	57.58	0.20	1.87	0.29	22.39	0.32	7.28	3.55
P16-02	14-20	Tailing	8.86	0.12	63.95	0.15	2.34	0.36	16.99	0.27	7.15	3.73
P16-03	24-30	Tailing	12.57	0.17	59.93	0.25	3.47	0.55	13.34	0.35	10.23	3.63
P16-04	34-40	Natural	25.93	0.31	20.50	0.50	0.44	0.17	38.27	0.94	13.93	2.79
P16-05	54-60	Natural	21.36	0.34	23.26	0.41	0.56	0.20	41.62	0.83	12.49	2.84
P16-06	74-80	Natural	16.35	0.26	20.83	0.42	0.31	0.12	52.81	0.71	8.84	2.84

(Continued)

TABLE 1 Continued

Core	Interval (cm)	Class	Al_2O_3 (%)	CaO (%)	Fe_2O_3 (%)	MgO (%)	MnO (%)	P_2O_5 (%)	SiO_2 (%)	TiO_2 (%)	LOI (%)	True Density (g/cm^3)
P16-07	94-100	Natural	14.64	0.24	19.12	0.39	0.27	0.11	57.06	0.69	8.17	2.82
P16-08	114-120	Natural	19.36	0.27	24.06	0.41	0.44	0.16	44.20	0.67	11.15	2.88
P19-01	04-08	Tailing	8.96	0.16	49.47	0.14	0.93	0.18	34.40	0.32	5.61	3.41
P19-02	16-20	Tailing	11.46	0.19	45.82	0.22	1.60	0.28	32.76	0.42	7.42	3.33
P19-03	28-32	Tailing	9.61	0.13	58.84	0.17	2.14	0.35	21.54	0.31	7.20	3.66
P19-04	40-44	Tailing	11.98	0.19	55.18	0.22	3.18	0.51	19.49	0.36	9.41	3.56
P19-05	50-54	Tailing	12.76	0.25	53.92	0.24	3.04	0.50	19.45	0.37	10.05	3.50
P19-06	60-64	Natural	7.36	0.23	17.65	0.23	0.40	0.10	68.77	0.55	3.83	2.88
P19-07	74-78	Natural	7.95	0.25	13.63	0.22	0.11	0.07	72.48	0.57	3.56	2.82
P19-08	88-92	Natural	6.52	0.19	10.66	0.18	0.06	0.05	78.20	0.42	2.46	2.77
P19-09	100-106	Natural	22.44	0.17	10.65	0.43	0.36	0.08	51.90	0.97	11.22	2.71
P19-10	110-116	Natural	24.07	0.16	10.49	0.40	0.41	0.09	51.89	0.96	11.53	2.71
P22-01	0-10	Tailing	19.07	0.28	36.64	0.34	1.21	0.26	31.38	0.66	11.48	3.05
P22-02	10-20	Tailing	17.64	0.26	38.48	0.30	1.29	0.27	30.21	0.63	11.36	3.11
P22-03	30-38	Natural	22.56	0.34	20.79	0.42	0.49	0.20	42.59	0.88	12.64	2.80
P22-04	54-62	Natural	24.15	0.31	19.72	0.40	0.46	0.21	41.75	0.87	12.59	2.79
P22-05	74-80	Natural	19.98	0.29	20.80	0.41	0.37	0.16	47.42	0.86	10.36	2.85
P22-06	90-98	Natural	25.24	0.32	20.02	0.44	0.49	0.28	39.05	0.84	13.98	2.78
P22-07	114-120	Natural	24.50	0.37	19.25	0.46	0.45	0.18	42.05	0.94	12.58	2.81
P22-08	130-136	Natural	24.68	0.30	20.46	0.41	0.40	0.19	40.88	0.93	12.69	2.82
P22-09	150-154	Natural	9.52	0.20	22.05	0.30	0.15	0.08	61.78	0.78	4.69	2.93

In this context, the geochemical assessment of sediments from the Paraopeba River must consider both the geological context and the history of human occupation (34).

The B1 dam iron tailings were studied prior to the B1 dam collapse by Gomes (35). He demonstrated that they were essentially composed of hematite and quartz, in addition to kaolinite and gibbsite in smaller proportions, and defined the average chemical composition of the tailings as being dominated by iron oxide (48%) and silica (20.6%), followed by aluminum and manganese oxides (2.5% and 1.0%, respectively). Importantly, the mineral beneficiation processes at the Córrego do Feijão mine did not involve metallurgical or concentration processes; only physical segregation associated with grain size reduction was performed. Hence, the main mineralogical and chemical characteristics of the tailings were inherited from the iron ores without subtraction or addition of other components.

The B1 dam collapse caused profound and long-lasting changes in the Paraopeba River basin, affecting various environmental, hydrological, and social aspects. Among the main environmental impacts are the contamination of sediments and water, alterations to fluvial morphology, and the reduction of the river's self-purification capacity. Analyses of specific density and mineral content data (11) and Fe/Al and Mn/Al ratios (12) have demonstrated that the influence of tailings in bedload sediment is geographically restricted to the reach between the mouth of Ferro-Carvão creek and the weir built over the main channel near the Igarapé Thermoelectric Plant (Figure 1). This few-meter-high spillway deaccelerates sediment transport and slows tailing propagation below the thermoelectric dam (36–38 39).

3 Materials and methods

3.1 Sampling

A vibracorer sampling device was employed to collect bottom sediments and/or tailings from the river channel during the 2019 dry season. The drilling was conducted using a 5-meter-long, 3-inch-diameter stainless steel vibracoring system. To minimize material loss during core retrieval—especially of finer-grained fractions such as clay and silt—a catcher device was installed at the base of the corer.

The study area includes a nonaffected sampling point located upstream from the Ferro-Carvão creek mouth on the Paraopeba River (M2 in Figure 1). Fifty-four samples were selected from 6

cores following the Brazilian National Guide for Sampling and Sample Preservation (40). Samples were crushed to a particle size of less than 1.00 mm, quartered, pulverized, dried at 100°C, and subsequently submitted for analysis. Core logs, sample descriptions and mineral content can be found at Laureano et al. (11).

3.2 X-ray fluorescence

The concentrations of major and minor elements (Al_2O_3, CaO, Fe, MgO, Mn, P, SiO_2, and TiO_2) were determined using wavelength-dispersive X-ray fluorescence (WD-XRF) spectroscopy. Analyses were conducted on a PANalytical Axios Minerals sequential XRF spectrometer, operating at 2.4 kW of power, and equipped with a Rhodium (Rh) anode X-ray tube (maximum voltage: 60 kV; maximum current: 50 mA; window thickness: 75 µm Be). Both flow and scintillation detectors were used during measurements. All analyses were performed at the Vale Mineral Development Center (CDM) in Minas Gerais, Brazil. For the purpose of this research, the concentrations of Fe, Mn and P were stoichiometrically converted to their oxide forms, Fe_2O_3, MnO and P_2O_5, respectively.

3.3 Density

The true density of samples was measured by a helium gas displacement ultra-pycnometer (Quantachrome Instruments ULTRAPYC 1200e). This analysis considers only the mass of solid constituents, excluding voids or pores within the material.

3.4 Data analysis

The results obtained were statistically processed in Excel on the Windows 10 operating system. Boxplots, scatterplots, and Pearson correlation analyses were performed in Excel. Ternary diagrams were created using RStudio software, through specific functions provided by the ggtern package (41).

4 Results

4.1 Geochemical characteristics of tailings and natural sediments

Multiproxy analysis of mineralogical data conducted by Laureano et al. (11) demonstrated that tailings and natural sediments can be distinguished by different proportions of hematite, quartz, and kaolinite. The whole-rock geochemical analyses of major and minor elements in the natural sediment samples and tailings, which were previously classified in the aforementioned study, are presented in Table 1.

There is a remarkable contrast in chemical composition between the sediments and tailings, with the former being generally enriched in Al_2O_3, SiO_2, CaO, MgO, and TiO_2 and impoverished in Fe_2O_3 and, to a minor degree, in MnO and P_2O_5, compared with the tailings, which have markedly higher true density values than the sediments. The loss on ignition (LOI) values ranged from 0.75% to 14.9% in the natural sediment samples and from 1.0 to 11.5% in the tailings samples (Table 1). From upstream to downstream in the Paraopeba River, the Fe_2O_3 contents of the tailings samples tended to decrease, with an increase in SiO_2 and, most importantly, Al_2O_3 as the Al-silicate content in the sample increased.

The values of Fe_2O_3 and true density allow a clear separation between tailings and sediments, as shown by a graphical analysis of the dispersion of true density data as a function of the concentration of Fe_2O_3 (Figure 2) obtained for the global set of tailings and natural sediment samples. Pearson's correlation coefficients (R) were obtained using a confidence limit of a=95%. A moderate linear adjustment (R^2 = 0.63), according to Newbold's (1995) criterion, was found between these 2 variables for the natural sediment samples, whereas a strong linear correlation (R^2 = 0.98) was observed for the tailing samples.

For a clear distinction of sediments and tailings, as required for restoration purposes of the impacted area, it is crucial, from a compositional perspective, to define the signatures of the studied materials, with a focus on their chemical constituents and the relationships between them, with the aim of determining those capable of acting as traceable materials (42). In this sense, considering that the tailings from B1 and natural sediments have mineralogical compositions that are clearly distinct from each other in most of the studied samples, a strong contrast in the chemical compositions of the sediments and tailings should also be expected, as observed in Table 1.

Thus, a comparison of the chemical compositions of such materials, presented below, was performed to identify potential tracer elements for distinguishing tailings and sediments on the basis of the whole-rock major and minor element data. The variations in all the analyzed whole-rock parameters of the samples of natural sediments and tailings are compared on the basis of boxplot diagrams (43) (Figure 3), and Table 2 shows basic statistical data.

Fe_2O_3 and SiO_2 - According to Table 1; Figure 3, the concentrations of Fe_2O_3 in the tailings samples were almost universally higher than those in the natural sediment samples. Except for the maximum content (41%) recorded in sample M2-08, the iron concentrations (1.1% to 29.3%) in the natural sediments are below the concentration range (36.6% to 88.8%) observed in the tailings. Conversely, all the silica concentrations (38.3% - 94.1%) in the natural sediment are higher than the concentration range (8.4% - 30.4%) observed in the tailings. These findings highlight the notable difference in iron oxide mineral contents between the tailings and the natural sediments, as described by Laureano et al. (11). Therefore, the Fe_2O_3 and SiO_2 contents are considered potential tracers for distinguishing between tailings from B1 and natural sediments from the Paraopeba River.

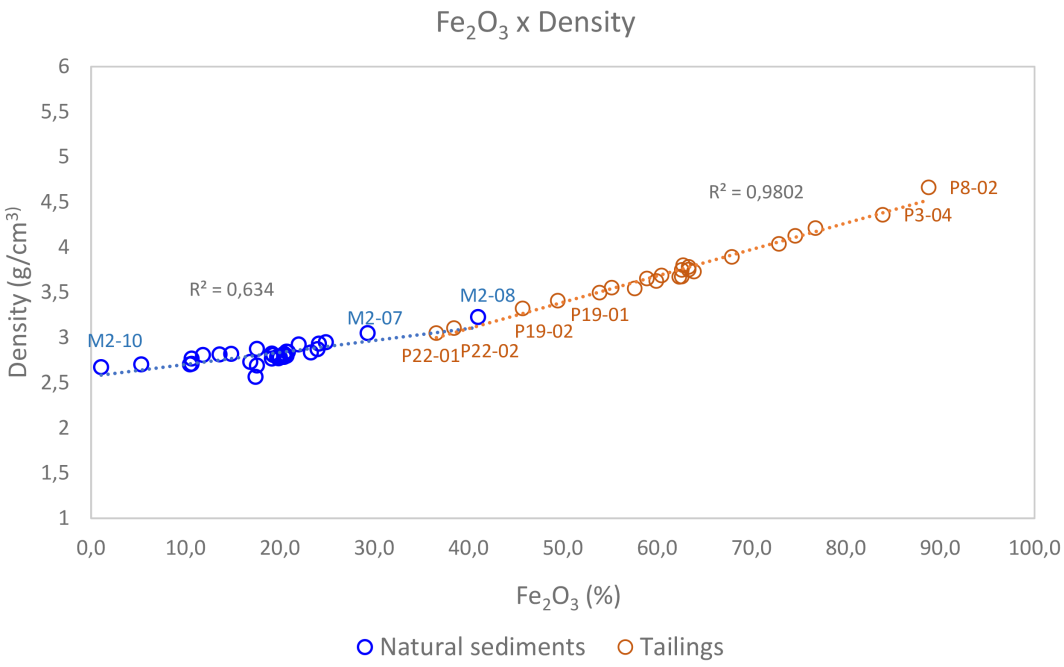

FIGURE 2
Data dispersion of true density versus Fe_2O_3 concentration for natural sediments and B1 tailings.

Al_2O_3 – Compared to the SiO_2 concentrations, the Al_2O_3 concentrations did not exhibit a similar sum effect of mineralogical composition. Despite the median value (8.0%) in the tailing samples being approximately half the median value (15.9%) in the natural sediments (Figure 3), the Al_2O_3 concentration range from P25 (8.6%) – P75 (23.4%) overlapped most of the range observed in the natural sediments [i.e., from the minimum value (2.5%) to P75 (23.4%)]. Therefore, Al_2O_3 can only be considered a possible tracer for distinguishing tailings from natural sediments if it is combined with other components, including SiO_2.

MnO - MnO concentrations are generally higher and show significantly greater variability in tailings (0.32% to 3.46%) than in natural sediments (0.01 to 0.56%) (Table 2, Figure 3). The first concentration quartile in the tailings samples (0.32% to 0.59%) partially overlap with the third and fourth quartiles (0.36% to 0.56%) in the natural sediments. Owing to the relatively small overlap between the concentrations of tailings and natural sediments, if combined with other elements from whole-rock analysis, Mn is considered a potential tracer for distinguishing tailings and sediments.

In addition to the variations in the modal contents of kaolinite, quartz and hematite in tailings and sediments, which resulted in a robust mineralogical fingerprint for the distinction of these materials, Laureano et al. (11) also suggested the modal contents of Mn oxides as tailings indicators. However, Mn oxides also occur as an accessory mineral in natural sediments. For this reason, the Mn contents are not always conclusive, and Mn is considered here as a potential chemical tracer for the separation of tailings and sediments, as are the other minor elements, Ti, Ca, Mg, and P.

CaO and MgO – The CaO values obtained via total rock analysis ranged from 0.09% to 0.37% in the natural sediments and from 0.04% to 0.28% in the tailings samples (Table 2). Similarly, the MgO concentrations ranged from 0.10% to 0.50% and from 0.02% to 0.34%, respectively. These results revealed a significant overlap between the different element concentrations. In both cases, at least 50% of the concentrations in the natural sediments overlapped with the corresponding concentrations in the tailings (Figures 3, 4). Owing to these overlaps, Ca and Mg alone do not constitute good chemical tracers for distinguishing natural sediments from tailings.

TiO_2 – TiO_2 also shows significant overlap in concentration ranges between the natural sediments and tailings. The upper quartile of TiO_2 concentrations from the tailings was superimposed up to approximately the concentration of the natural sediment sample P30 (Figure 3). Hence, Ti alone also does not present a satisfactory potential tracer for natural sediments, especially tailings, considering the whole-rock composition.

P_2O_5 – P_2O_5 also show significant overlap between natural sediments and tailings. The first and second quartiles (0.08% to 0.26%) of the tailings contents overlap with the second quartile to the maximum value (i.e., 0.07% to 0.28% P_2O_5) of the sediment contents (Figure 3). Consequently, P_2O_5 does not show satisfactory potential for use as a tailings tracer.

In the ternary diagram of Fe–Si–Al (Figure 4A), the natural sediment and tailings samples plot in two clearly distinct fields because of the contrasting enrichments of Fe_2O_3 in the tailing samples and silica in the natural sediments. The relationship between the chemical composition and dominant mineralogical phases of the analyzed samples is evident (Figure 4A). The highest

10.3389/fsoil.2025.1617526

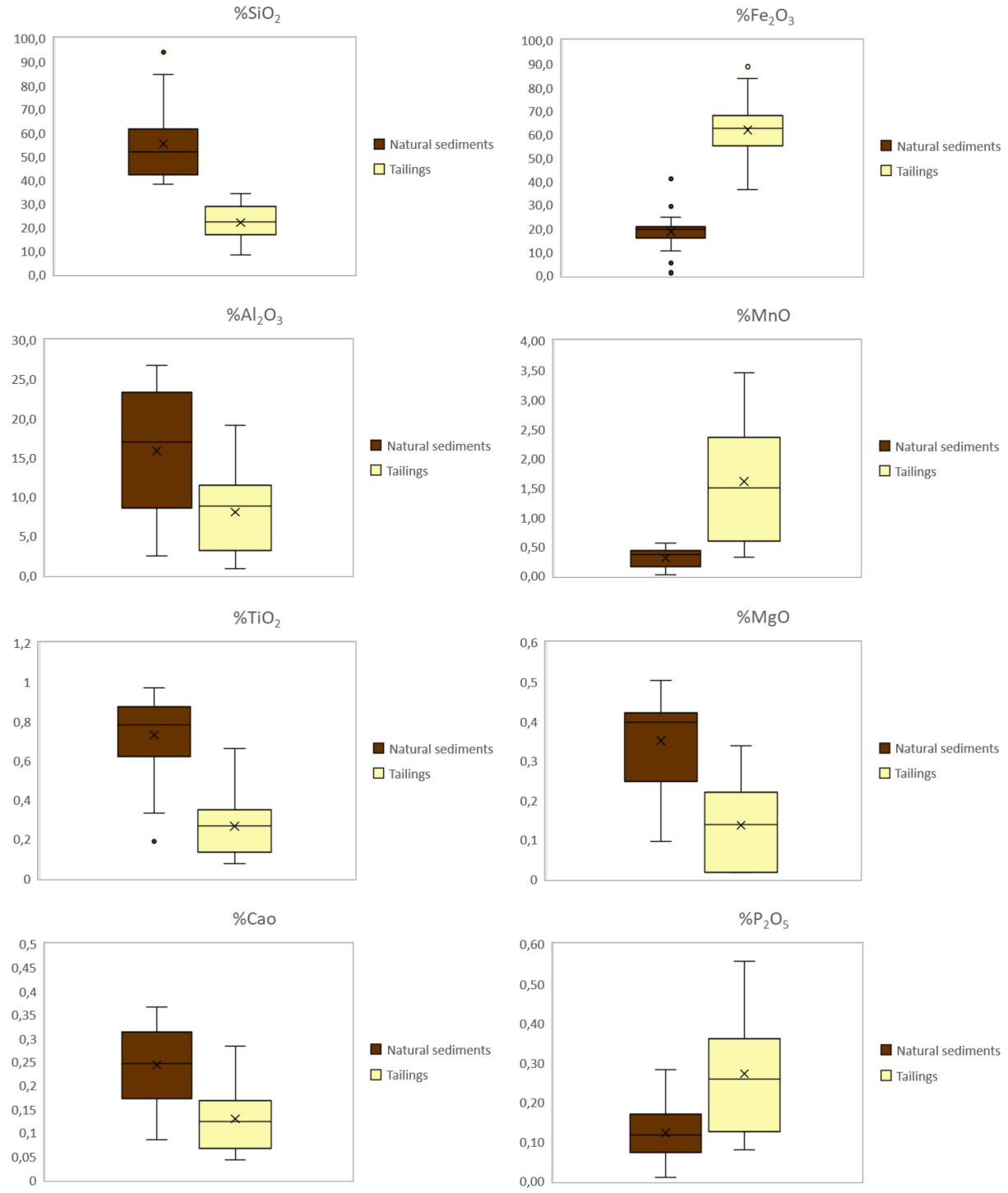

FIGURE 3
Major and minor element concentration boxplots of natural sediments from the Paraopeba River and B1 tailings ($N_{sediment}$ = 31; $N_{tailing}$ = 23).

concentrations of SiO_2 correspond to natural sediments composed predominantly of quartz (Qz) associated with or not associated with hematite (Qz+Hm). The samples with high concentrations of Fe_2O_3 are tailing samples dominated by Fe oxides (Hm and Hm>). Finally, the samples with relatively high concentrations of Al_2O_3 and moderate contents of Fe_2O_3 and SiO_2 are mostly natural sediments and have high modal contents of kaolinite.

Unlike other minor elements, such as Ca, Mg, and Ti, which are typically associated with the natural sediment mineral composition, Mn has been used as a tracer for tailings present in water and

10.3389/fsoil.2025.1617526

TABLE 2 Basic statistical parameters of the whole-rock data ($N_{sediment}$ = 31; $N_{tailings}$ = 23).

Element	Class	Mean	StanDev	Min	Q1	Median	Q3	Max
Al_2O_3	Sediment	15.87	7.94	2.47	7.95	17.04	24.07	26.79
	Tailing	8.03	5.14	0.87	3.15	8.86	11.46	19.07
CaO	Sediment	0.24	0.08	0.09	0.17	0.25	0.31	0.37
	Tailing	0.13	0.07	0.04	0.07	0.12	0.17	0.28
Fe_2O_3	Sediment	18.64	7.19	1.10	14.85	19.72	20.83	41.10
	Tailing	61.83	12.61	36.64	55.18	62.56	67.87	88.72
MgO	Sediment	0.35	0.11	0.10	0.24	0.40	0.42	0.50
	Tailing	0.14	0.10	0.03	0.03	0.14	0.22	0.34
MnO	Sediment	0.31	0.15	0.01	0.15	0.36	0.43	0.56
	Tailing	1.61	1.09	0.32	0.59	1.49	2.34	3.47
P_2O_5	Sediment	0.12	0.06	0.01	0.07	0.12	0.17	0.28
	Tailing	0.27	0.16	0.08	0.12	0.26	0.36	0.56
SiO_2	Sediment	55.40	15.21	38.27	42.05	51.88	61.78	94.06
	Tailing	21.95	7.22	8.44	16.99	22.31	28.85	34.40
TiO_2	Sediment	0.73	0.20	0.19	0.61	0.78	0.88	0.97
	Tailing	0.27	0.16	0.07	0.14	0.27	0.35	0.66

sediments after the B1 dam failure (25). The possibility of using oxides of minor elements as discriminants between natural sediments and tailings was evaluated by constructing the diagram 10*MnO – 10*(CaO + MgO + TiO_2) – Fe_2O_3 (Figure 4B). A 10-fold factor was applied to Mn and (CaO + MgO + TiO2) for better resolution in the diagram. The compositional difference between tailings and natural sediments is also evident in that plot, with the natural sediments being enriched in (CaO + MgO + TiO_2) and generally impoverished in MnO compared with the tailing samples. The relationship between chemical composition and dominant modal mineralogy can be observed in Figure 4B. Notably, the samples enriched in kaolinite, mostly natural sediments, are also enriched in MnO.

The data points representing natural sediments and tailings samples are concentrated in two distinct fields, indicating a compositional contrast between the natural sediments and the tailings. Higher concentrations and greater dispersion of (CaO +MgO+TiO_2) characterize natural sediments, whereas compared

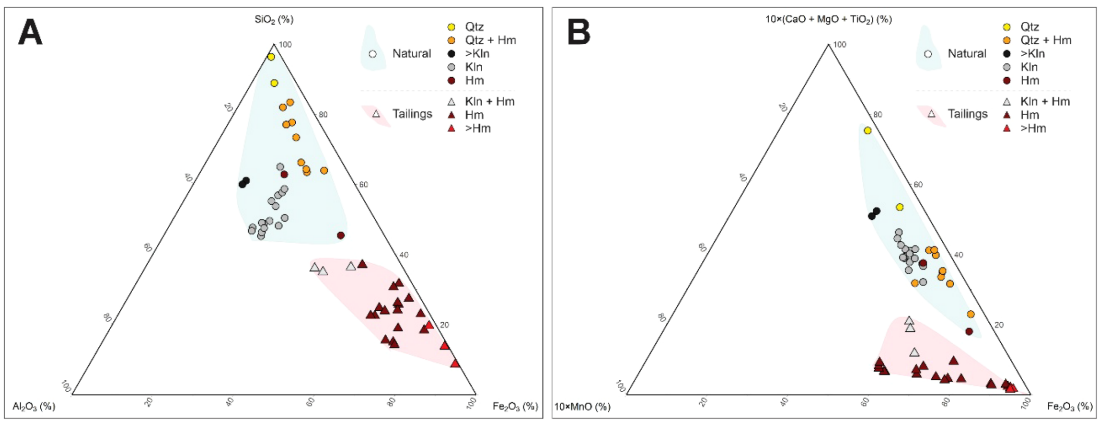

FIGURE 4
(A) Ternary diagram of SiO_2 × Al_2O_3 × Fe_2O_3: whole-rock composition (Table 1) vs. modal mineral content (11); **(B)** Ternary diagram 10*(CaO+MgO +TiO_2) × 10*MnO × Fe_2O_3: whole-rock composition (Table 1) vs. modal mineral composition (11).

TABLE 3 Basic statistics of the tailings and natural sediment indices (samples from the 2019 drilling campaign).

Material type	Index	Minimum	P10	P25	Median	P75	P90	Maximum
Natural sediments	IRS1	0.004	0.05	0.07	0.11	0.12	0.14	0.24
	IRS2	0.028	0.07	0.1	0.16	0.2	0.22	0.25
Tailings	IRS1	0.24	0.28	0.42	0.47	0.54	0.65	0.79
	IRS2	0.44	0.51	0.64	0.74	0.78	0.8	0.82

with the natural sediment samples, the tailings samples are characterized by higher contents and greater variability of MnO and Fe_2O_3.

4.2 Tailings–sediments indices (IRS from the acronym in Portuguese: Índice Rejeito-Sedimento)

As a function of the results presented in the previous sections, two ratios were considered for distinguishing between tailings and sediments in the study area: (i) Fe_2O_3 concentrations versus Al_2O_3 and SiO_2 concentrations and (ii) MnO concentrations versus TiO_2, CaO, and MgO concentrations (Table 1). Below, Equations 1, 2 are proposed with the objective of numerically identifying and summarizing the chemical contrasts between tailings samples originating from B1 and the natural sediment samples from the Paraopeba River, enabling the distinction of these materials.

$$IRS1 = [Fe2O3]/\{[Fe2O3] + [Al2O3] + [SiO2]\} \quad (1)$$

$$IRS2 = [MnO]/\{[MnO] + [TiO2] + [CaO] + [MgO] \quad (2)$$

In Equations 1, 2, either elementary concentrations or oxides can be used. Equations 1, 2 were applied to the 2019 dataset (Table 1). According to Equations 1, 2, the higher the relative concentrations of Fe and Mn are, the higher the values of the IRS1 and IRS2 indices are, respectively, with the maximum value tending to 1 (Table 3). On the other hand, higher concentrations of $[Al] + [Si]$ *or* $[Ti] + [Ca] + [Mg]$ result in lower IRS1 and IRS2 indices, with the minimum value tending to zero. Consequently, the tailings samples have relatively high IRS1 values of 0.24 to 0.79 and IRS2 values of 0.44 to 0.82 (Table 3), whereas the natural sediments have maximum IRS1 and IRS2 values of 0.24 and 0.25, respectively. The IRS1 values range from 0.004 to 0.24 in the natural sediment samples and from 0.24 to 0.79 in the tailings samples. The medians are 0.11 and 0.47, respectively. Similarly, the IRS2 values range from 0.03 to 0.25 in the natural sediment samples and from 0.44 to 0.82 in the samples. The medians are 0.16 and 0.74, respectively. The distributions of the IRS1 and IRS2 populations are shown in Figure 5. For both indices, there is essentially no overlap between the populations corresponding to the samples interpreted as natural sediments and tailings. This is consistent with the mineralogical and density contrasts observed between these two materials (11).

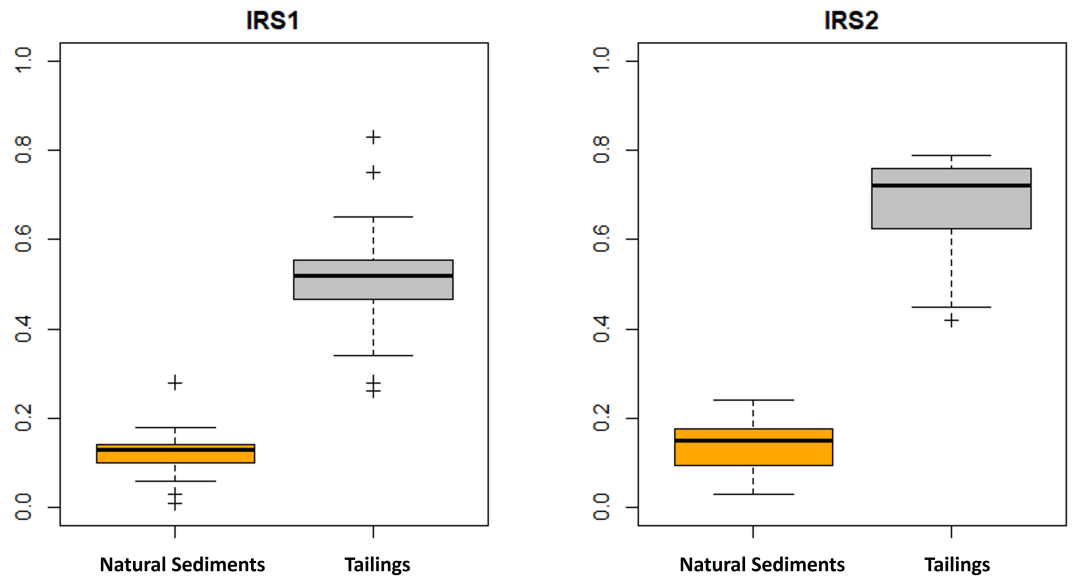

FIGURE 5
Distribution of IRS1 **(A)** and IRS2 **(B)** values, elementary concentrations. Data from the 2019 drilling program (Table 1).

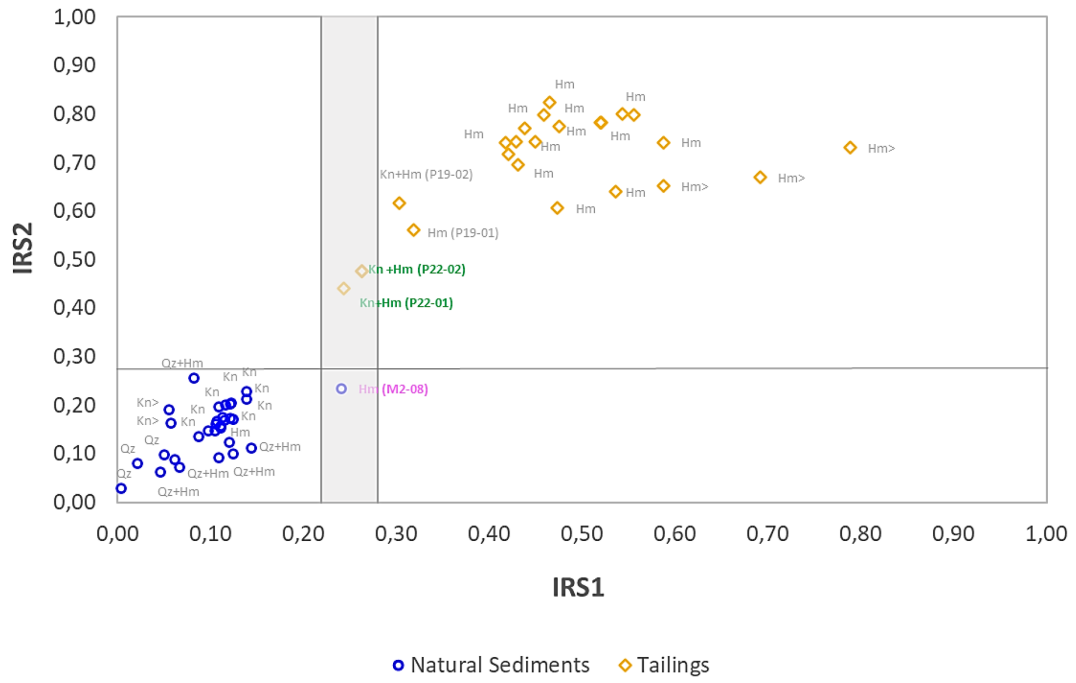

FIGURE 6
IRS1 x IRS2 (elementary concentrations) dispersion graph for natural sediments from the Paraopeba River and transported tailings from the B1 dam. The gray area indicates the uncertainty zone with possibly mixed samples of both materials. Data from the 2019 drilling program (Table 1).

In an IRS1 versus IRS2 scatterplot (Figure 6) based on the chemical data (Table 1) associated with dominant mineralogical phases (11), the combined effect of relatively higher contents of [Fe] versus [Si] and [Al] in the IRS1 index and the relatively higher contents of [Mn] versus [Ti], [Ca], and [Mg] in the IRS2 index resulted in a diagonal distribution of the natural sediments and tailings samples. The IRS1 and IRS2 values for the natural sediments generally plot in the first quadrant, close to the origin. Data from the tailings samples are distributed far from the natural sample data and plot generally in the third quadrant. The lines of separation between the four fields were defined arbitrarily in the diagram, following the best data adjustment (Figure 6).

Despite the remarkable separation between most of the tailings and natural sediment samples, an uncertainty zone (shaded) was created in Figure 6. In this zone, the values of IRS1 and IRS2 between samples of the different materials are very close. Samples of both the natural sediment (M2-08) and the tailings (P22-01) share an IRS1 value of 0.24. Sample P22-02, with an IRS1 value of 0.26, which was correlated with the tailings, also plots in this uncertainty zone. Sample M2–08 has a density and Fe_2O_3 concentration close to the lower limits of these parameters observed in the tailings (Table 1); however, this sample has an IRS2 index that is consistent with that of natural sediments (Figure 6). Samples P22–01 and P22–02 have Fe_2O_3 and Al_2O_3 contents, respectively, which are lower and higher than the dominant values in the tailings. These discrepancies can be explained by the presence of high modal kaolinite in these samples (Figures 4A, B). High modal kaolinite generally implies enrichment in MnO (44), which was observed in these samples (Table 1; Figure 4B) and is a characteristic feature of tailings. Given the aforementioned aspects, the lower threshold of IRS1 in the tailings and the higher threshold of IRS2 in the natural sediments serve as benchmarks for discussing the feasibility of utilizing the defined indices for distinguishing between natural sediments and tailings.

5 Discussion

The results presented above indicate that the IRS1 and IRS2 indices perform satisfactorily in distinguishing between natural sediments and tailings deposited in the Paraopeba River, based on sediment core samples. However, considering the existence of several studies focused on the characterization of Paraopeba River sediments affected by the tailings, the objective of this section is to evaluate the applicability of the IRS1 and IRS2 indices to independent datasets and to discuss the specific characteristics observed in each case.

The indices were applied to stream sediments from the Paraopeba River sampled during 2019, within the scope of the Emergency Monitoring Program (45). The objective was to test whether the indices are able to distinguish samples associated with tailings from those derived from unaffected natural sediments (Figure 7).

The IRS graphical tool revealed that the samples collected upstream of the UTE (Thermal power plant) Igarapé spillway presented high values of IRS1 and IRS2 and spread within the tailing field. On the other hand, the samples collected downstream

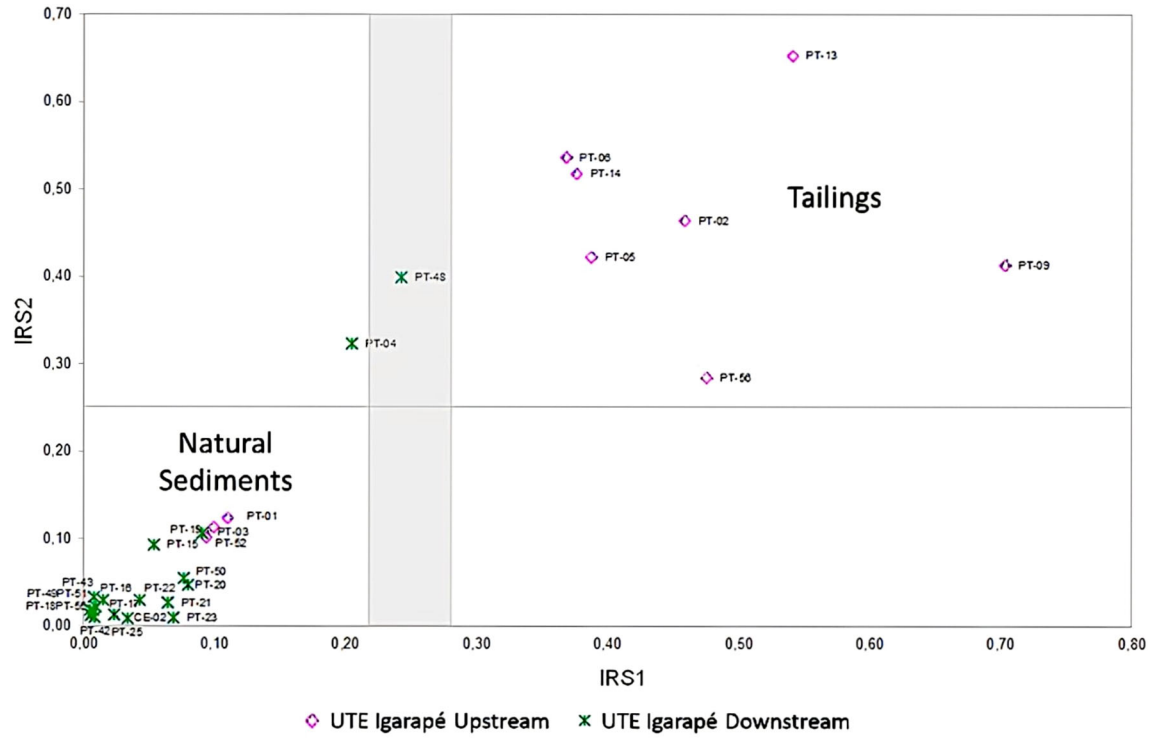

FIGURE 7
Diagram of IRS1 versus IRS2 (elementary concentrations) for samples collected along the Igarapé UTE adapted from Arcadis (45).

of the spillway presented lower indices values and were mostly distributed in the first quadrant, indicating a geochemical resemblance to natural sediments.

Several authors have shown the importance of the spillway in tailings propagation (36–39). Different approaches have shown that it has deaccelerated sediment transport and slowed the propagation of tailings downstream of the dam. One should also account for the tailings' density, which ranges from 3.11 to 4.67 g/cm^3 and is considerably greater than that of natural sediments (11). This helps promote tailings deposition behind the spillway, hindering their advance downstream.

The data from the other three sampling points deserve special attention; all of them plot in the natural sediment field despite being located upstream of the spillway (Figure 7). PT-52 presents a coherent result with its spatial context since it is located upstream of the Ferro Carvão creek mouth and constitutes a reference for stream sediment quality monitoring. Its IRS1 × IRS2 position reflects its provenance as sediment not affected by tailings. On the other hand, PT-01 and PT-03 are located in a river sector that has been impacted by tailings, but they are clearly under the influence of a dredging system built to remove mining waste from the river. It is plausible to assume that their IRS1 x IRS2 positions reflect the renewal of the active bedload strata.

PT04 and PT48 plot within the uncertainty area of the diagram (Figure 7), which remains to be explained. They are located downstream but not far from the spillway, and their IRS1 × IRS2 positions probably reflect a mixing effect corresponding to tailing samples enriched in kaolinite (11) because of the high content of Mn but lower Fe concentration in relation to Si (Figures 4A, B).

The IRS1 vs. IRS2 diagram was also applied to test sediments sampled by Silva et al. (18) within the Paraopeba River channel (Figure 8). Those samples were collected downstream (samples J1, J2, and J3, with J3 being closest to the impact site and J1 being the farthest from it) and upstream (samples M4.1 and M4.2) from the confluence of Ferro Carvão Creek (Figure 1). The authors considered the concentrations of Mn in the downstream samples elevated and assumed them to be influences of tailings from the B1 dam. On the other hand, the sediments sampled upstream from Ferro Carvão Creek presented relatively low concentrations of Fe and Mn and were considered representative of natural sediments. They concluded that samples J1, J2, and J3 were impacted by tailings.

According to their IRS values, all five samples analyzed by Silva et al. (18) plot in the natural sediment field, including those sampled in the affected area (Figure 1). Samples J1, J2, and J3 have Fe_2O_3 and MnO concentrations ranging from 16.2% to 29.2% for Fe_2O_3 and 0.2% to 0.3% for MnO (Table 4), which are lower than the minimum values obtained for the tailings samples in this study (Table 2). These concentrations result in low values for IRS1 and IRS2, thereby justifying the classification of these samples as natural sediments according to the indices. As discussed before, renewing of the active bedload layer has been noted since 2019 because of fluvial dynamics and dredging in most proximal river trenches. Silva et al. (18) collected samples four years after the B1 dam collapsed and neglected dredging activities. Four years is enough time to mix and/

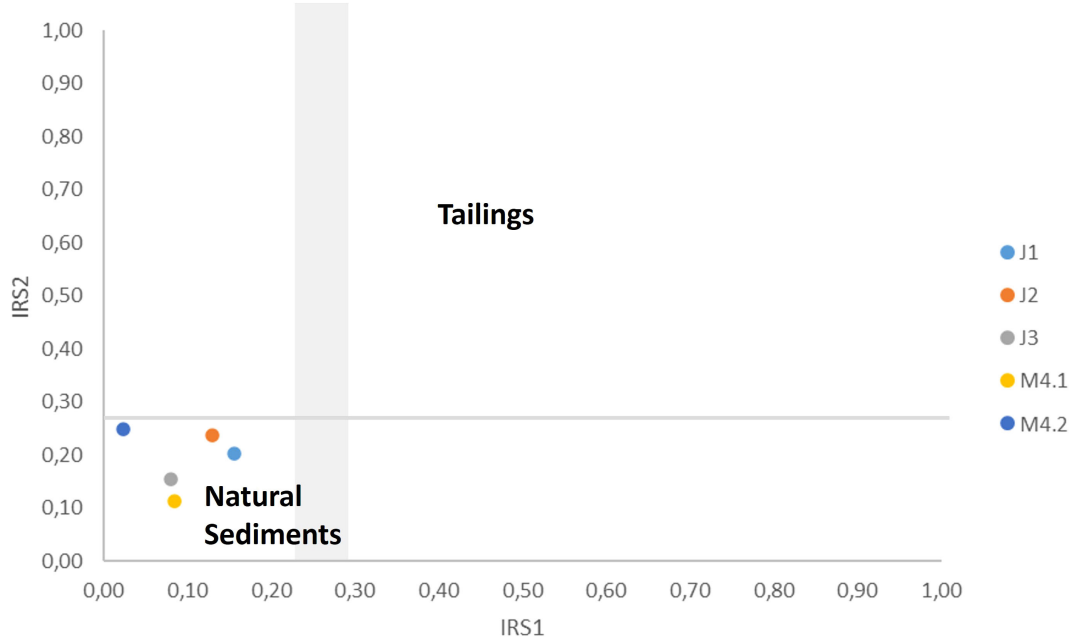

FIGURE 8
IRS1 vs. IRS2 (elementary concentrations) plot for samples from the area of confluence between Ferro do Carvão Creek and the Paraopeba River. Chemical data from Silva et al. (18).

or cover tailings deposits, calling into question the assumption that tailings samples are still there be sampled.

The indices are also suitable for testing the identification of tailings in overbank locations after flood events. Tailings and tailings-derived contaminants can deposit and accumulate in floodplains after mine dams burst (46–48). Recent work has attempted to assess the environmental effect of the presence of iron mine tailings on soils in an alluvial context (49–51), but it would be valuable to have a geochemical signature capable of revealing the presence of tailings in the environment instead of relying only on visual descriptions in the field. Macklin et al. (47) argued that because of natural availability and historical mining activities, major accidents occur where the background levels of metals and contaminants are already high.

Dos Reis et al. (8) observed that anomalous metal concentrations in a section affected by tailings are primarily related to the regional geological context. Similarly, Quaresma et al. (52) observed the enrichment of fine particles, increased turbidity, and elevated metal concentrations on the southeastern Brazilian continental shelf following the collapse of a dam in Minas Gerais state, Brazil. Although they reported changes in grain size composition and metal enrichment, the authors also noted pre-existing contributions prior to the event, which, according to them, complicates the distinction between post-collapse deposits and natural sediments. This finding reinforces the importance of developing geochemical indices capable of distinguishing natural sediments from tailings, based on a fast and low-cost methodology. Furthermore, because sediment quality guideline values are rare worldwide, understanding the mineral content and geochemical baseline is a key factor for the success of environmental investigations and restoration efforts.

6 Conclusions

In addition to differences in modal mineralogy and density, there is a marked chemical contrast between the natural sediments of the Paraopeba River and the tailings released by the B1 dam collapse. These compositional differences provide an opportunity to assess the presence and distribution of tailings within the alluvial sediments. This is especially relevant in contexts where the

TABLE 4 Whole-rock chemical analyses of sediments from the Paraopeba River by Silva et al. (18).

Sample	SiO2	Fe2O3	Al2O3	K2O	MgO	MnO	CaO	Na2O	P2O5	LOI
J1	53.7	29.2	9.6	0.8	0.3	0.2	0.2	0.2	0.1	5.2
J2	52.1	23.6	12.5	0.9	0.4	0.3	0.2	0.2	0.1	8.8
J3	63.5	16.2	11.0	1.1	0.4	0.2	0.3	0.3	0.1	6.1
M4.1	71.7	18.2	4.9	0.8	0.3	0.1	0.2	0.2	0.1	2.6
M4.2	89.9	5.8	2.2	0.7	0.1	0.1	0.1	0.2	0.03	0.8

geological setting and the legacy of long-term mining activities have already contributed to elevated background levels of metals and other potentially toxic elements, making it challenging to clearly recognize and quantify the specific impacts of the dam failure on sediment composition.

The IRS1 and IRS2 indices developed in this study have demonstrated a strong ability to distinguish tailings from natural sediment samples within the Paraopeba River basin. One of the key strengths of these indices lies in their derivation from a simple and low-cost analytical methodology — X-ray fluorescence (XRF) — which is widely available in commercial laboratories around the world. This accessibility makes the approach easily applicable in various environmental assessment scenarios globally.

Unlike traditional sediment quality assessments, which typically rely on the determination of trace element concentrations, the methodology proposed in this study focuses on differences in mineralogical composition and major oxide contents. This approach is particularly suitable for scenarios involving tailings dam failures, where one of the main concerns is monitoring the physical dispersion of tailings along the river course, rather than solely assessing trace metal contamination.

While there are other robust and well-established techniques available in the literature for sediment characterization, the IRS indices offer the added advantage of rapid calculation from routine XRF data, allowing for fast and reliable distinction between sediment classes. This provides timely and actionable information to support environmental impact assessments and decision-making processes.

Given the large volume of data typically generated by monitoring programs associated with dam decommissioning or failure response, the IRS indices — along with the graphical tools developed in this study — hold significant potential for tracking tailings dispersion both spatially and temporally across affected river systems.

Data availability statement

The original contributions presented in the study are included in the article/supplementary material. Further inquiries can be directed to the corresponding author.

Author contributions

FP: Writing – original draft, Writing – review & editing. FL: Writing – review & editing, Writing – original draft. CC: Writing – review & editing, Writing – original draft. GS: Writing – original draft, Writing – review & editing. RD: Writing – review & editing, Writing – original draft. VP: Writing – review & editing, Writing – original draft. LL: Writing – review & editing, Writing – original draft.

Funding

The author(s) declare that no financial support was received for the research and/or publication of this article.

Conflict of interest

Author FP was employed by the company SRK Consulting. Authors FL and VP were employed by the company Vale S.A.

The remaining authors declare that the research was conducted in the absence of any commercial or financial relationships that could be construed as a potential conflict of interest.

Generative AI statement

The author(s) declare that no Generative AI was used in the creation of this manuscript.

Publisher's note

References

1. Lottermoser B, Lottermoser BG. Sulfidic mine wastes. *Mine Wastes: Character. Treat Environ Impacts*. (2010), 43–117.

2. Protasio FNM, de Avillez RR, Letichevsky S, de Andrade Silva F. The use of iron ore tailings obtained from the Germano dam in the production of a sustainable concrete. *J Cleaner Product*. (2021) 278:123929.

3. Kossoff D, Dubbin WE, Alfredsson M, Edwards SJ, Macklin MG, Hudson-Edwards KA. Mine tailings dams: Characteristics, failure, environmental impacts, and remediation. *Appl Geochem*. (2014) 51:229–45.

4. Sánchez LE, Alger K, Alonso L, Barbosa FAR, Brito MCW, Laureano FV. Impacts of the Fundão Dam failure, A pathway to sustainable and resilient mitigation. In: *Rio Doce Panel Thematic Report No1*. IUCN, Gland, Switzerland (2018). doi: 10.2305/IUCN.CH.2018.18.en

5. Lima RE, de Lima Picanço J, da Silva AF, Acordes FA. An anthropogenic flow type gravitational mass movement: the Córrego do Feijão tailings dam disaster, Brumadinho, Brazil. *Landslides*. (2020) 17:2895–906.

6. Bird G, Hudson-Edwards KA, Byrne P, Macklin MG, Brewer PA, Williams RD. River sediment geochemistry and provenance following the Mount Polley mine tailings spill, Canada: The role of hydraulic sorting and sediment dilution processes in contaminant dispersal and remediation. *Appl Geochem*. (2021) 134:105086.

7. Liu J, Li Y, Zhang B, Cao J, Cao Z, Domagalski J. Ecological risk of heavy metals in sediments of the Luan River source water. *Ecotoxicology*. (2009) 18:748–58.

8. Dos Reis DA, Nascimento LP, De Abreu AT, Nalini Junior HA, Roeser HMP, da Fonseca Santiago A. Geochemical evaluation of bottom sediments affected by historic mining and the rupture of the Fundão dam, Brazil. *Environ Sci pollut Res*. (2020) 27:4365–75.

9. Owens PN, Petticrew EL, Albers SJ, French TD, Granger B, Laval B, et al. Annual pulses of copper-enriched sediment in a North American river downstream of a large lake following the catastrophic failure of a mine tailings storage facility. *Sci Total Environ*. (2023) 856:158927.

10. Orlando MTD, Rangel CVGT, Galvao ES, Orlando CGP, Bastos AC, Quaresma VS. *Characterization of Sediments from the Fundao Dam Failure*. Sao Paulo: Blucher (2019) 16. doi: 10.5151/wcacem-01

11. Laureano FV, Kwitko-Ribeiro R, Guimarães L, Leão LP. Mineralogical fingerprint of iron ore tailings in Paraopeba River bedload sediments after the B1 dam failure in Brumadinho, MG (Brazil). *Minerals*. (2022) 12:716.

12. Pacheco FAL, do Valle Junior RF, de Melo MMAP, Pissarra TCT, de Melo MC, Valera CA, et al. Prognosis of metal concentrations in sediments and water of Paraopeba River following the collapse of B1 tailings dam in Brumadinho (Minas Gerais, Brazil). *Sci Total Environ*. (2022) 809:151157.

13. Sun J, Zhao M, Cai B, Song X, Tang R, Huang X, et al. Risk assessment and driving factors of trace metal (loid) s in soils of China. *Environ pollut*. (2022) 309:119772.

14. Miller JR, Lechler PJ, Mackin G, Germanoski D, Villarroel LF. Evaluation of particle dispersal from mining and milling operations using lead isotopic fingerprinting techniques, Rio Pilcomayo Basin, Bolivia. *Sci Total Environ*. (2007) 384:355–73.

15. Valeriano CM, Neumann R, Alkmim AR, Evangelista H, Heilbron M, Neto CCA, et al. Sm–Nd and Sr isotope fingerprinting of iron mining tailing deposits spilled from the failed SAMARCO Fundão dam 2015 accident at Mariana, SE-Brazil. *Appl Geochem*. (2019) 106:34–44.

16. Xu Z, Belmont P, Brahney J, Gellis AC. Sediment source fingerprinting as an aid to large-scale landscape conservation and restoration: A review for the Mississippi River Basin. *J Environ Manage*. (2022) 324:116260.

17. Haddadchi A, Ryder DS, Evrard O, Olley J. Sediment fingerprinting in fluvial systems: review of tracers, sediment sources and mixing models. *Int J Sediment Res*. (2013) 28:560–78.

18. Silva LSC, de Lima Picanço J, Pereira CC, Silva D, de Almeida TN. Dispersion of tailings in the Paraopeba River system after Brumadinho dam failure: Brazil. *Environ Earth Sci*. (2024) 83:128.

19. TEC3 – Geotecnia e Recursos Hídricos. *Estudo Conceitual Mina Córrego do Feijão: Estimativa do volume de rejeitos depositado em trechos do Rio Paraopeba em decorrência do rompimento da barragem B-I*. Relatório Técnico T19098-026-RE–Rev.1. Belo Horizonte (2020).

20. Vergilio CDS, Lacerda D, Oliveira BCVD, Sartori E, Campos GM, Pereira ALDS, et al. Metal concentrations and biological effects from one of the largest mining disasters in the world (Brumadinho, Minas Gerais, Brazil). *Sci Rep*. (2020) 10:5936.

21. Parente CE, Lino AS, Carvalho GO, Pizzochero AC, Azevedo-Silva CE, Freitas MO, et al. First year after the Brumadinho tailings' dam collapse: Spatial and seasonal variation of trace elements in sediments, fishes and macrophytes from the Paraopeba River, Brazil. *Environ Res*. (2021) 193:110526.

22. Kobayashi H, Garnier J, Mulholland DS, Quantin C, Haurine F, Tonha M, et al. Exploring a new approach for assessing the fate and behavior of the tailings released by the Brumadinho dam collapse (Minas Gerais, Brazil). *J Hazardous Mater*. (2023) 448:130828.

23. Quintarelli JM, da Silva Junior GC, Viglio EP. A note on the influence of the mine tailings released in the córrego do feijão mine disaster on the water bodies of brumadinho, minas gerais, Brazil. *Mine Water Environ*. (2023) 42:187–99.

24. Sardinha DS, Pinto MS, Menezes PHBJ, Brucha G, Silveira JT, Godoy LH, et al. Major, Trace and Rare Earth Elements Geochemistry of Bottom Sediments in the Retiro Baixo Reservoir after the B1 Tailings Dam Rupture, Paraopeba River (Brazil). *Minerals*. (2024) 14(6):621. doi: 10.3390/min14060621

25. Pacheco FAL, do Valle Junior RF, de Melo MMAP, Pissarra TCT, de Souza Rolim G, de Melo MC, et al. Geochemistry and contamination of sediments and water in rivers affected by the rupture of tailings dams (Brumadinho, Brazil). *Appl Geochem*. (2023) 152:105644.

26. Matos F, Dias R. A Gestão dos Recursos Hídricos em MG e a Situação da Bacia Hidrográfica do Rio Paraopeba. *Gestão Regionalidade*. (2012) 28(83).

27. Companhia de Pesquisa de Recursos Minerais – CPRM. *Boletins de Monitoramento - Bacia do Rio Paraopeba*. (2019). Available online at: http://www.cprm.gov.br/sace/index_rio_paraopeba.php. (Accessed July 22, 2024).

28. Baltazar OF, Zucchetti M. Lithofacies associations and structural evolution of the Archean Rio das Velhas greenstone belt, Quadrilátero Ferrífero, Brazil: A review of the setting of gold deposits. *Ore Geology Rev*. (2007) 32:471–99.

29. Rosière CA, Spier CA, Rios FJ, Suckau VE. The itabirites of the Quadrilátero Ferrífero and related high-grade iron ore deposits: an overview. (2008) 15.

30. Babinski M, Chemale F Jr., Van Schmus WR. The PB/PB age of the minas supergroup carbonate rocks, quadrilatero FERRIFERO, BRAZIL. *Precambrian Res*. (1995) 72:235–45.

31. MaChado N, Schrank A, Noce CM, Gauthier G. Ages of detrital zircon from Archean-Paleoproterozoic sequences: Implications for Greenstone Belt setting and evolution of a Transamazonian foreland basin in Quadrilátero Ferrífero, southeast Brazil. *Earth Planetary Sci Lett*. (1996) 141:259–76.

32. Alkmim FF, Marshak S. Transamazonian orogeny in the Southern Sao Francisco craton region, Minas Gerais, Brazil: evidence for Paleoproterozoic collision and collapse in the Quadrilátero Ferrıfero. *Precambrian Res*. (1998) 90:29–58.

33. Spier CA, de Oliveira SM, Sial AN, Rios FJ. Geochemistry and genesis of the banded iron formations of the Cauê Formation, Quadrilátero Ferrífero, Minas Gerais, Brazil. *Precambrian Res*. (2007) 152:170–206.

34. Leão LP, De Vicq R, Nalini HA Jr, Leite MGP. Mapeamento Geoquímico do Manganês e Avaliação da Qualidade de Sedimentos Fluviais e Águas Superficiais do Quadrilátero Ferrífero, Brasil. *Anuário do Instit. Geociências - UFRJ*. (2019) 42:444–55.

35. Gomes MA. Caracterização tecnológica no aproveitamento do rejeito de minério de ferro *[dissertation]*. Ouro Preto: Mineral Engineering Department of Federal University of Ouro Preto (2009).

36. Rotta LHS, Alcântara E, Park E, Negri RG, Lin YN, Bernardo N, et al. The 2019 Brumadinho tailings dam collapse: Possible cause and impacts of the worst human and environmental disaster in Brazil. *Int J Appl Earth Observ Geoinform*. (2020) 90:102119.

37. Garcia MH, Rojas AF. *Task 1: 1D – Sediment transport analysis for the Paraopeba River, final report V.1.0*. Ven Te Chow Hydrosustems Laboratory, University of Illinois, Technical report (2022). 116p.

38. Garcia MH, Fytanidis D. Task 4: 3D CFD modeling of hydraulic structures UTE igarapé. In: *Final report. Technical report* (2022). p. 35.

39. Terêncio DPS, Pacheco FAL, do Valle Junior RF, de Melo MMAP, Pissarra TCT, de Melo MC, et al. The Igarapé Weir decelerated transport of contaminated sediment in the Paraopeba River after the failure of the B1 tailings dam (Brumadinho). *Int J Sediment Res*. (2023) 38:673–97.

40. Companhia Ambiental do Estado de São Paulo - CETESB. "Guia nacional de coleta e preservação de amostras: água, sedimento, comunidades aquáticas e efluentes líquidos." In: *Guia nacional de coleta e preservação de amostras: água, sedimento, comunidades aquática e efluentes líquidos*. (2011). p. 325–5.

41. Hartmann K, Krois J, Rudolph A. *Statistics and Geodata Analysis using R (SOGA-R)*. Freie Universität Berlin: Department of Earth Sciences (2023). Avaible online at: https://www.geo.fu-berlin.de/en/v/soga-r/Advances-statistics/Multivariate-approaches/Factor-Analysis/End-member-modelling-analysis/The-EMMA-al.

42. Hoefs J, Hoefs J. *Stable isotope geochemistry* Vol. 285. Berlin: springer (2009).

43. Tukey JW. *Exploratory data analysis*. Reading, MA: Addison-wesley. (1977) 2:131–60.

44. Li F, Yin H, Zhu T, Zhuang W. Understanding the role of manganese oxides in retaining harmful metals: Insights into oxidation and adsorption mechanisms at microstructure level. *Eco-Environment & Health*. (2024) 3(1):89–106.

45. Arcadis. *Relatório Técnico - Relatório da qualidade da água superficial e sedimentos na bacia do rio Paraopeba. Relatório de Fechamento de Ciclo de Estiagem (janeiro/2019 a setembro/2020)*. Belo Horizonte, MG (2020).

46. Langedal M. The influence of a large anthropogenic sediment source on the fluvial geomorphology of the Knabeåna-Kvina rivers, Norway. *Geomorphology*. (1997) 19:117–32.

47. Macklin MG, Brewer PA, Hudson-Edwards KA, Bird G, Coulthard TJ, Dennis IA, et al. A geomorphological approach to the management of rivers contaminated by metal mining. *Geomorphology*. (2006) 79:423–47.

48. Lecce SA, Pavlowsky RT. Floodplain storage of sediment contaminated by mercury and copper from historic gold mining at Gold Hill, North Carolina, USA. *Geomorphology*. (2014) 206:122–32.

49. Batista ÉR, Carneiro JJ, Pinto FA, Dos Santos JV, Carneiro MAC. Environmental drivers of shifts on microbial traits in sites disturbed by a large-scale tailing dam collapse. *Sci Total Environ*. (2020) 738:139453.

50. Queiroz HM, Ying SC, Abernathy M, Barcellos D, Gabriel FA, Otero XL, et al. Manganese: The overlooked contaminant in the world largest mine tailings dam collapse. *Environ Int*. (2021) 146:106284.

51. Páez BCMD, Dias MDS, Severiano EDC, Carneiro MAC, Martins PCC. Limiting physical properties of Technosols formed by the Fundão dam failure, Minas Gerais, Brazil. *Rev Bras Ciec do Solo*. (2024) 48:e0230021.

52. Quaresma VS, Aguiar VMC, Bastos AC, Oliveira KS, Vieira FV, Sá F, et al. The impact of trace metals in marine sediments after a tailing dam failure: the Fundão dam case (Brazil). *Environ Earth Sci*. (2021) 80:1–16.